Heterogeneous Uptake of Ozone on Reactive Components of Mineral Dust Aerosol: An Environmental Aerosol Reaction Chamber Study

Praveen K. Mogili,[†] Paul D. Kleiber,[‡] Mark A. Young,*[,§] and Vicki H. Grassian*[,†,§]

Departments of Chemical and Biochemical Engineering, Physics and Astronomy, and Chemistry, The University of Iowa, Iowa City, Iowa 52242

Received: June 10, 2006; In Final Form: October 16, 2006

We have undertaken a kinetic study of heterogeneous ozone decomposition on α-Fe_2O_3 (hematite) and α-Al_2O_3 (corundum) aerosols under ambient conditions of temperature, pressure, and relative humidity in order to better understand the role of mineral dust aerosol in ozone loss mechanisms in the atmosphere. The kinetic measurements are made in an environmental aerosol reaction chamber by use of infrared and ultraviolet spectroscopic probes. The apparent heterogeneous uptake coefficient, γ, for ozone reaction with α-Fe_2O_3 and α-Al_2O_3 surfaces is determined as a function of relative humidity (RH). The uptake of ozone by the iron oxide surface is approximately an order of magnitude larger than that by the aluminum oxide sample, under dry conditions. At the pressures used, α-Fe_2O_3 shows clear evidence for catalytic decomposition of ozone while α-Al_2O_3 appears to saturate at a finite ozone coverage. The measured uptake for both minerals decreases markedly as the RH is increased. Comparison with other literature reports and the atmospheric implications of these results are discussed.

Introduction

The role of particulate matter in the atmosphere has elicited a great deal of recent interest due to the possible influence of heterogeneous interactions on the balance of trace gas species in the atmosphere and the consequent impact on global biogeochemical cycles.[1−7] Surface chemistry involving mineral dust species may be especially important as these crustal materials comprise a significant fraction of the total tropospheric aerosol mass loading.[7,8] Uptake by mineral dust surfaces may be a competitive loss pathway for various gas-phase species.[8−11] Heterogeneous surface chemistry followed by desorption processes could represent a significant source for other trace atmospheric gases. Heterogeneous chemical pathways involving mineral dust might be very different from the more well understood homogeneous cycles that are commonly included in atmospheric chemistry models. The surface-mediated pathways have the potential to be catalytic in nature, magnifying the influence of dust particles on atmospheric cycles. The chemical composition and physical properties of the dust aerosol can, in turn, be altered through processing in the atmosphere, leading to vastly different behavior as the aerosol mass is transported away from the source region.

Several field studies have found low ozone mixing ratios in regions of the atmosphere also containing high mass concentrations of mineral dust particulates.[9,12] Among the most notable examples of such an anticorrelation were the observations by de Reus et al.[9] in 1997 during the ACE-2 campaign in the vicinity of the Canary Islands. Through the use of a box model simulation, it was determined that including a pathway for the direct removal of ozone by mineral dust surface resulted in a maximum ozone depletion of 50%. While the model predictions were in accordance with observed mixing profiles from the field data, it was noted that any conclusions came with a large degree of uncertainty due to poor experimental characterization of O_3 uptake by mineral dust.

Previous Knudsen cell reactor studies from our laboratory have revealed the catalytic behavior of mineral aerosol in the destruction of ozone.[13,14] At ozone pressures of 8 ppb, we measured an uptake coefficient of $\gamma = (1.2 \pm 0.4) \times 10^{-4}$ for initial uptake of O_3 on α-Al_2O_3 and $\gamma = (2.0 \pm 0.3) \times 10^{-4}$ for α-Fe_2O_3. The apparent uptake decreased when the dust samples were exposed to ozone for long periods. However, ozone uptake was never completely saturated, indicating that the process is catalytic and active surface sites are regenerated. Knudsen cell studies are typically performed at low pressure under dry conditions with minimal water present, most likely as residual water adsorbed on the surface.[15] At relative humidity (RH) values relevant to the troposphere, the dust aerosol surface will be coated with water, which can impact the uptake and surface reaction process.[16] Other surface coatings, both organic and inorganic in nature, can also influence ozone interactions with dust aerosol.[16]

Hanisch and Crowley[17] also investigated Saharan dust using a Knudsen cell and reported an uptake coefficient of $\gamma \approx 10^{-5}$ at 30 ppb exposure to ozone. They found that the dust surface eventually saturated and became inactive to further ozone decomposition. If the dust sample was subject to vacuum for long periods, however, some recovery of activity toward ozone decomposition was observed. The effects of RH were not explored in this work.

Abbatt and co-workers[18−20] have studied ozone decomposition on alumina and authentic Saharan dust samples and have further explored the influence of RH on the kinetics. The initial uptake coefficient for O_3 on α-Al_2O_3 films was found to be $\gamma \approx 10^{-6}$ at initial ozone concentration of 10^{14} cm^{-3} (≈4 ppm) and increased by an order of magnitude with an order of magnitude lower ozone concentration.[18] The Saharan dust sample exhibited

* Authors to whom correspondence should be addressed.
[†] Department of Chemical and Biochemical Engineering.
[‡] Department of Physics and Astronomy.
[§] Department of Chemistry.

10.1021/jp063620g CCC: $33.50
Published on Web 12/05/2006

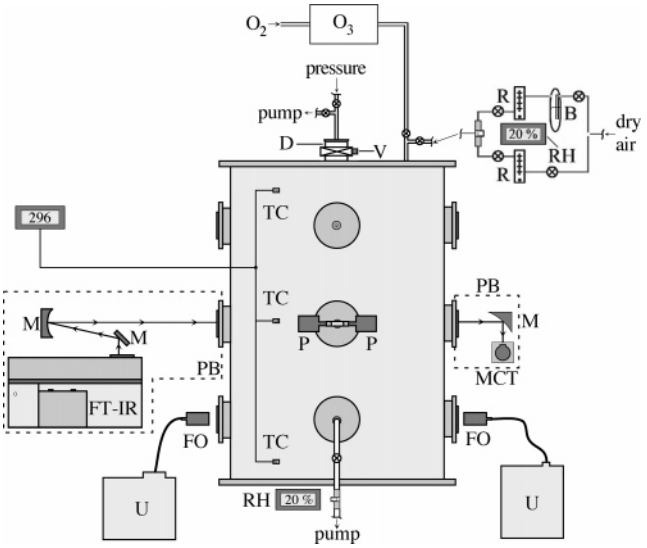

Figure 1. Schematic diagram of the atmospheric chamber and associated instrumentation showing the pressurized dust sample chamber (D) and valve (V); water bubbler (B), flow meters (R), and relative humidity sensors (RH); FT-IR spectrometer (FT-IR), mirrors for the external IR beam (M), mid-band HgCdTe IR detector (MCT), and purge boxes for the external beam path (PB); UV/vis spectrometer (U) and fiber optic collimators (FO); thermocouples (TC) and pressure transducers (P); and the ozone generator (O_3).

a lower uptake, $\gamma \approx 2 \times 10^{-7}$, also at ozone concentrations of 10^{14} cm^{-3}.[19] The measured uptake coefficient was reported to be independent of the RH, up to 75%, in the case of either sample.[18,19] A subsequent study utilized an infrared (IR) spectroscopic probe to monitor the growth of a spectral feature on alumina films assigned to a surface oxide product of the reaction with ozone.[20] The rate constant for growth of the surface product was found to decrease significantly as the RH was increased up to values of nearly 25%, in contrast to the previous results.

A static reaction cell was used to measure an uptake coefficient of $\gamma \approx 3 \times 10^{-10}$ for ozone on α-Al_2O_3 at higher O_3 pressures, from 200 to 8000 ppm, but the measured uptake was found to be pressure-independent over this range.[21] These studies were done on dried samples but the authors note that water adsorption prevented ozone decomposition by the alumina.

Related studies of RH dependence have not been reported for α-Fe_2O_3 (hematite), a relatively reactive metal oxide component of mineral dust. In addition, previous experiments have largely relied on powder samples where interparticle interactions and voids can complicate the analysis. The present studies are intended to more fully understand the effect of mineral dust on the concentration of ozone in the atmosphere under relevant conditions. The studies utilize an aerosol reaction chamber and spectroscopic probes to maintain isolated particle conditions. A full range of RH conditions is explored to evaluate the effect on ozone uptake, and a comparison is made between iron oxide and alumina samples.

Experimental Section

A schematic diagram of the environmental aerosol chamber, which has been described previously,[22] is shown in Figure 1. The chamber is a stainless steel cylinder with a total volume of 0.15 m^{-3} and a surface to volume ratio of 10.7 m^{-1}. The interior surfaces of the chamber and sealing flanges are coated with FEP Teflon and all chamber connections are fabricated from either Teflon or glass to achieve a chemically inert environment, minimizing losses due to wall reactions. The large flanges that seal the top and bottom of the chamber and four sets of side arms provide access to the chamber interior for sample introduction, a mechanical pump, pressure and RH measurement, and the various instrumental probes.

Two different spectroscopic instruments were utilized to monitor ozone concentrations inside the reaction chamber; a Fourier transform infrared (FT-IR) spectrometer (Mattson Infinity 60 AR) and a fiber-optic-based UV/vis absorption spectrometer (Ocean Optics, SD2000). The IR beam is coupled through the chamber in a single-pass configuration by a series of gold-coated mirrors and then focused with an off-axis parabolic mirror onto an external liquid-nitrogen-cooled MCT detector. The chamber side arms are sealed with germanium windows to reduce complications associated with the reactivity of more common salt windows. The external IR beam path, including all mirrors and the detector, are continuously purged with dry air from a commercial gas generator (Whatman, 75−62). In the present configuration, the output of the purge air generator, humidified to the desired level, was also used to provide buffer gas for the chamber. The UV/vis spectrometer is coupled into the chamber through quartz windows by use of large-diameter collimation and collection optics. The UV/vis probe beam path is perpendicular to the IR beam but on the same horizontal plane.

In a typical experiment, the chamber is evacuated to a base pressure of 10 mTorr. Ozone is produced by flowing oxygen (Air Products, USP grade) through an electric discharge generator (OREC, Model O3V5-O) and into the chamber until the desired pressure is reached. Air from the purge generator is either used directly or first humidified to fill the chamber to a total pressure of 1 atm. The RH is approximately adjusted by use of a solid-state humidity sensor but the final determination is made via a Beer's law calibration of the measured IR absorbance of water vapor along with the chamber temperature. The error in RH was typically 1−2%, and the driest conditions obtained corresponded to a RH value of ≤1%. The chamber contents are allowed to sit for approximately 1−2 h in order to quantify wall losses. Powdered dust samples are rapidly introduced into the chamber through a pressurized sample line. A nozzle and impactor plate in the flow path ensure efficient deagglomeration of the sample, and the mixing time of the chamber contents is less than a minute. The powder is typically held under vacuum for 3 h prior to the experiment to remove as much residual water as possible.

The ozone concentration is constantly monitored with one or both of the spectroscopic probe instruments. The absorbance of the Hartley band at 254 nm is used to quantify the ozone concentration in the UV/vis experiments through a Beer's law calibration. The reported cross section at 254 nm is 1141×10^{-20} cm^2.[23] A typical spectrum is shown in Figure 2 for 8 ppm O_3. In the IR, the absorbance at 1054 cm^{-1} is similarly used to measure concentration where the absorptivity has been measured to be 3.74×10^{-4} ppm^{-1} m^{-1} at a total pressure of 1 atm.[24,25] In Figure 3A, a portion of a typical IR spectrum is shown for the chamber contents with 40 ppm O_3 prior to the introduction of the aerosol sample. The UV/vis probe is more sensitive than the FT-IR, with a detection limit of approximately 1 ppm of ozone. Temporal resolution of the probe spectrometers was approximately 2 min for the settings used in the current experiments.

α-Fe_2O_3 (Aldrich) and α-Al_2O_3 (Alfa Aesar) dust samples were obtained from commercial sources. An automated multipoint Brunauer−Emmett−Teller (BET) analysis (Quantochrome

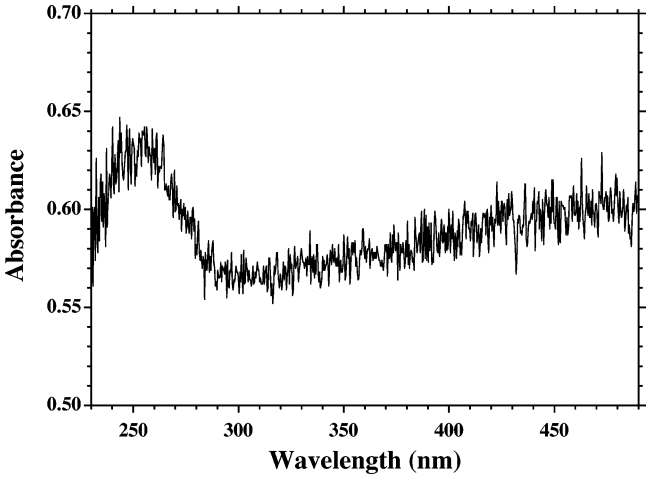

Figure 2. Typical UV−vis spectrum of 8 ppm of ozone in the presence of α-Fe_2O_3 and humidified air showing the 254 nm Hartley band of O_3.

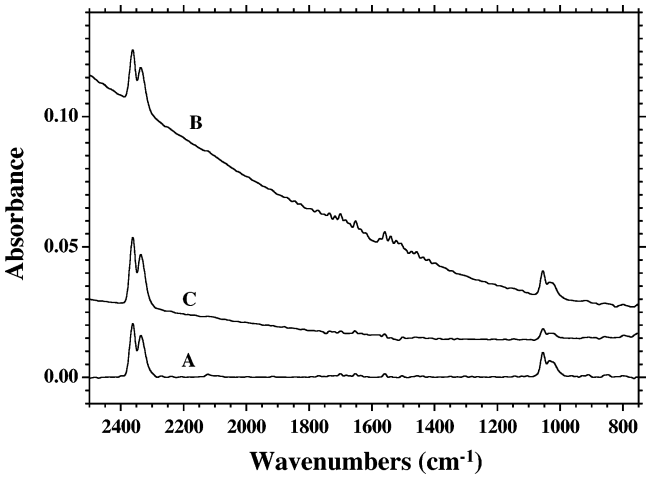

Figure 3. (A) Portion of the IR spectrum showing the chamber contents before aerosol introduction at 32% RH and 40 ppm O_3. The feature at 1043 cm^{-1} is due to O_3, and the 2342 cm^{-1} band is CO_2. (B) Spectrum recorded a few minutes after introduction of the aerosol. The sloping baseline is due to Mie extinction by the suspended particles. (C) Spectrum similar to the one in panel B but recorded after a long reaction time. A decrease in the ozone band is evident. Water features have been subtracted and the spectra offset for clarity.

1700) was used to determine BET specific surface areas of 2.8 and 8.4 $m^2\ g^{-1}$ for α-Fe_2O_3 and α-Al_2O_3, respectively. The mass of each oxide (typically in the range of 1−4 g) was adjusted so that the total surface area in the chamber was approximately the same. An X-ray analysis was performed to confirm the mineral form of the iron oxide as α-Fe_2O_3 (hematite) and the aluminum oxide as α-Al_2O_3 (corundum).

Results

Two sets of experiments were performed for the ozone−hematite system. The FT-IR spectrometer was used to monitor the kinetics of ozone decay at higher initial pressures of O_3, in the range of 35−40 ppm. In order to investigate the influence of smaller initial ozone concentrations, and consequent lower surface coverage of the hematite, the more sensitive UV/vis probe was employed to study ozone pressures in the range of 3−8 ppm. Some typical IR spectral data are shown in Figure 3 for an experiment at 32% RH. The spectra have been shifted vertically and gas-phase water absorptions have been subtracted from the data for clarity. The data in Figure 3A show a region

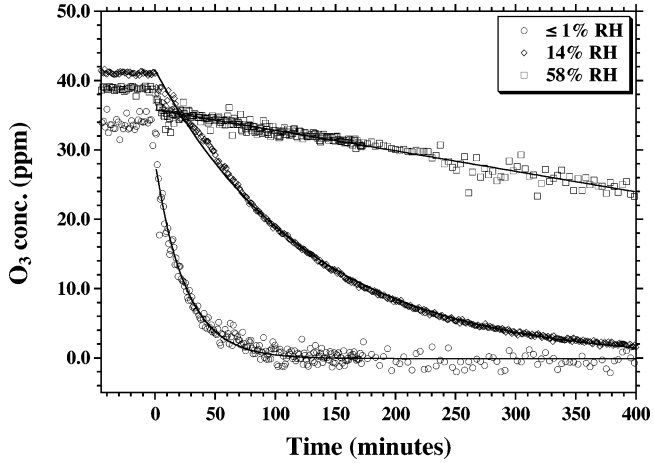

Figure 4. Ozone decay as a function of time for the α-Fe_2O_3 system at several RH values, measured with the FT-IR probe. Solid lines are fits to the data by use of an exponential function.

of the IR spectrum prior to introduction of the aerosol sample. The ozone band centered at 1043 cm^{-1} is clearly visible, along with an absorption due to trace CO_2 at 2342 cm^{-1} that originates from the ozone sample line. The spectrum of Figure 3B was collected a few minutes after the α-Fe_2O_3 aerosol was introduced and exhibits a sloping baseline characteristic of Mie scattering by the suspended particles. Finally, Figure 3C represents a reaction time of several hours and shows that the ozone band has decreased in intensity, signifying reactive loss due to the presence of the mineral dust. The CO_2 band does not appear to change in intensity. No absorbance features were observed to grow in with time over the IR spectral range of 5000−650 cm^{-1}, indicating that any gaseous product species are IR-inactive.

The IR data show that ozone is lost from the gas phase upon exposure to α-Fe_2O_3. The absorbance of the band maximum at 1054 cm^{-1} was used to quantify the ozone partial pressure as a function of time, as discussed (vide supra). The RH of the buffer gas was varied, up to about 60%, in order to investigate the influence of atmospheric water on the ozone loss kinetics. The time course data from several such experiments are shown in Figure 4. Under dry conditions, ≤1% RH, the ozone decreases relatively rapidly, exhibiting characteristic first-order kinetics with a time constant of about 25 min. All of the ozone is consumed over the course of the experiment and there is no saturation of the α-Fe_2O_3 surface under these conditions. Increasing the RH to 14% has a clear effect, resulting in a much slower loss of gaseous ozone although virtually all of the initial O_3 has reacted by the end of the experiment. At 58% RH, the suppression of ozone loss is even more marked, with a decay that is almost linear on the time scale represented in Figure 4, and only a fraction of the initial ozone has reacted by 400 min. In all instances, the loss subsequent to aerosol introduction is significantly larger than that for negative reaction times (i.e., before the dust is admitted into the chamber) and wall losses are inconsequential.

The kinetics of ozone loss can be modeled as a simple adsorption/reaction process with a rate constant, k:[22]

$$O_3 + S \xrightarrow{k} P \qquad (1)$$

where S represents the available surface sites in the reactor volume, and P represents reaction product species, either adsorbed or gas phase. Reaction 1 can be characterized in terms of a heterogeneous uptake coefficient, γ, which is the fraction of gas−surface collisions that lead to successful reaction.

TABLE 1: Ozone Uptake Coefficients on Mineral Dust Aerosol at Different RH Values[a]

O_3 pressure (ppm)	RH (%)	γ	T_N	$\gamma_{wet}/\gamma_{dry}$
		α-Fe_2O_3, High Pressure		
27	≤1	$(1.0 \pm 0.3) \times 10^{-7}$	2.00	1.00 ± 0.35
39	5	$(5.9 \pm 1.5) \times 10^{-8}$	2.93	0.56 ± 0.20
39	14	$(2.2 \pm 0.5) \times 10^{-8}$	3.14	0.21 ± 0.07
30	23	$(1.2 \pm 0.3) \times 10^{-8}$	2.25	0.12 ± 0.04
35	32	$(5.7 \pm 1.4) \times 10^{-9}$	2.87	0.054 ± 0.019
34	41	$(4.4 \pm 1.1) \times 10^{-9}$	2.46	0.042 ± 0.015
36	58	$(2.5 \pm 0.6) \times 10^{-9}$	2.63	0.024 ± 0.008
		α-Fe_2O_3, Low Pressure		
7.5	≤1	$(5.0 \pm 1.2) \times 10^{-8}$	0.58	1.00 ± 0.35
7.0	5	$(5.8 \pm 1.4) \times 10^{-8}$	0.52	1.2 ± 0.4
8.0	15	$(2.5 \pm 0.6) \times 10^{-8}$	0.64	0.51 ± 0.3
9.5	21	$(2.0 \pm 0.5) \times 10^{-8}$	0.74	0.41 ± 0.02
7.0	28	$(9.0 \pm 2.3) \times 10^{-9}$	0.50	0.18 ± 0.06
3.0	43	$(9.0 \pm 2.3) \times 10^{-9}$	0.22	0.18 ± 0.06
		α-Al_2O_3		
39	≤1	$(3.5 \pm 0.9) \times 10^{-8}$	0.94	1.00 ± 0.35
43	19	$(4.5 \pm 1.1) \times 10^{-9}$	0.83	0.13 ± 0.05
48	56		0.54	

[a] Errors in the reported uptake coefficients are estimated at 25% based on multiple experiments under similar conditions. The initial ozone pressure is classified as "high" for the IR experiments or "low" for the UV/vis experiments. The turnover numbers, T_N, are calculated as detailed in the text. The ratio of the uptake at higher RH values to that determined for the dry experiment, $\gamma_{wet}/\gamma_{dry}$, is also reported for each set of initial ozone pressures.

Assuming pseudo-first-order conditions, γ can be determined from

$$\gamma = \frac{4}{\bar{c} S_{BET} \tau [C_{mass}]} \quad (2)$$

where $\bar{c}$ is the mean speed of ozone (meters per second), C_{mass} is the mass concentration of the dust sample (grams per cubic meter), and S_{BET} is the specific surface area of the dust (square meters per gram), previously measured by a BET analysis. The characteristic decay time, $\tau = 1/k$, in eq 2 is determined from the fit of an exponential function to the ozone time course data. The solid lines in Figure 4 represent the results of such fits. The calculated uptake coefficients for a range of RH values are summarized in Table 1.

The reactivity of the hematite surface toward the heterogeneous decomposition of ozone can be characterized in terms of a turnover number, T_N:

$$T_N = \frac{\text{number of } O_3 \text{ molecules lost}}{\text{number of available surface sites}} \quad (3)$$

The total number of available hematite surface sites is calculated from the measured dust mass and the BET surface area, by use of a surface site density for α-Fe_2O_3 of 4.8×10^{14} sites cm^{-2}.[26] To calculate the number of ozone molecules that would be consumed, we extrapolated the fits of the data to long (infinite) times. A turnover number of $T_N > 1$ suggests that the surface is not saturated and that the process is catalytic, involving the regeneration of active surface sites. In the case of the dry experiment, Figure 4, all of the initial O_3 is lost to the surface, leading to a turnover number of 2.0. Turnover numbers for all of the experiments at different RH values are listed in Table 1. Since the calculated value of T_N is dependent on the available O_3 concentration under these conditions, values for the initial ozone pressure for each experiment are also contained in Table 1.

The effect of initial ozone concentration on the uptake kinetics and the RH dependence were investigated by using the more sensitive UV/vis probe technique. The results of monitoring the 254 nm band of O_3, as discussed (vide supra), for several RH values are shown in Figure 5. Similar to the case for the IR experiments, O_3 under dry conditions is observed to decompose upon exposure to the hematite surface and all of the initial ozone has reacted by experiment's end. As the RH is increased inside the chamber, ozone uptake is inhibited, and for the 28% RH data in Figure 5, there is still some O_3 remaining. These results are analogous to the outcome of the higher pressure IR probe experiments.

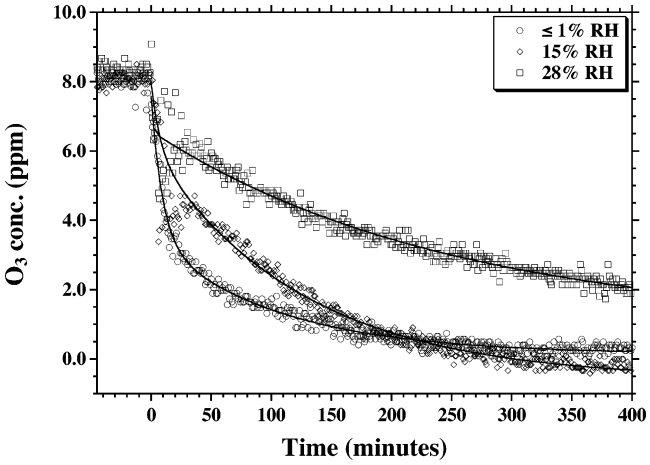

Figure 5. Ozone decay as a function of time for the α-Fe_2O_3 system at several RH values, measured with the UV/vis probe. Solid lines are fits to the data by use of an exponential function.

Fits to the data, shown by the solid lines in Figure 5, are applied to extract values for the uptake coefficient by use of eq 2, and the resultant values are tabulated in Table 1, along with calculations of the turnover numbers. For these reduced O_3 pressure experiments, the turnover numbers are less than unity, even for lower RH where all of the ozone is consumed.

The uptake coefficients reported in Table 1 were the result of fits to the data with a single-exponential function. However, the O_3 decay curves for RH data below about 20% were fit slightly better to a dual-exponential function. The implication is that there may be site heterogeneity on α-Fe_2O_3 that yields a fast initial decay, with a larger γ value, that rapidly saturates at low surface coverages. The data for ≤1% RH yield an uptake coefficient of approximately 2×10^{-7} for the fast initial decay,

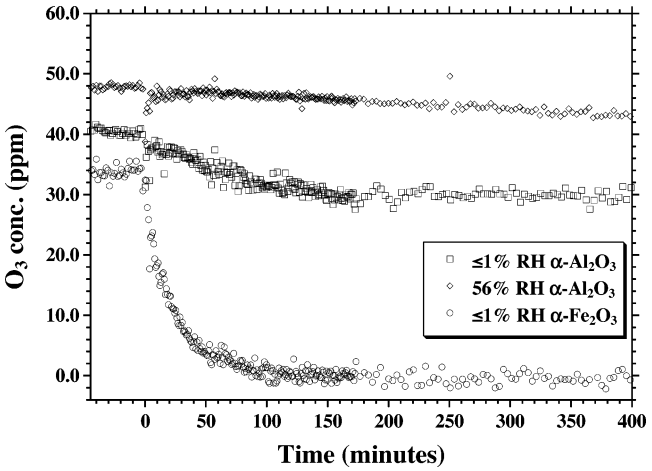

Figure 6. Comparison of the ozone decay on hematite and alumina dust aerosol at several RH values. The mass has been adjusted such that both samples have approximately the same available surface areas.

about 4 times larger than the value of γ reported in Table 1. Furthermore, the fraction of O_3 that is lost via this fast pathway accounts for only about 10% of the total consumption under dry conditions, rapidly decreases to a few percent with a RH of 15%, and is not clearly distinguishable at all at higher RH. The turnover number corresponding to the fast initial uptake is only $T_N \approx 0.07$ at $\leq 1\%$ RH.

Several experiments were conducted to make a comparison between α-Fe_2O_3 and α-Al_2O_3 for uptake of gaseous O_3. These studies were done with the FT-IR probe (higher O_3 pressures) and representative results are shown in Figure 6. The mass of powder used in each experiment was adjusted so that the total surface area of hematite and alumina was approximately equal, and as a consequence, the decay curves in Figure 6 can be directly compared. Under dry conditions, ozone uptake onto α-Fe_2O_3 is much more rapid than for the α-Al_2O_3 surface and the uptake coefficient is about 3 times smaller for the alumina sample. In addition, the ozone loss process saturates on the alumina surface, reaching a maximum turnover number of $T_N \approx 1$ at RH values of $\leq 1\%$. The α-Al_2O_3 sample is similar to α-Fe_2O_3 in that an increase in RH leads to a suppression of the ozone uptake, as evidenced by the 56% RH data shown in Figure 6. The 56% RH time course data for α-Al_2O_3 were not well fit by a single exponential and the decay was essentially linear on the time scale of the experiment. Analysis of the α-Al_2O_3 data is also contained in Table 1. A site density of 4×10^{14} sites cm^{-2} was used to calculate the turnover numbers in Table 1.[27]

While we are able to quantify the ozone concentration and the available BET surface area with a high degree of precision, the calculated turnover numbers depend on knowledge of the active surface site density, which potentially introduces some uncertainty. To address this, several experiments were performed with a high ratio of ozone molecules to surface sites by increasing the ozone pressure, reducing the powder mass and, hence, surface area introduced into the chamber, or a combination of both methods. These experiments were performed with the FT-IR to probe the reaction extent. For hematite samples, reducing the powder mass to about 0.4−0.7 g yielded turnover numbers from 25 to >40, with all of the ozone being consumed by the end of the experiment, even for initial O_3 pressures of 100 ppm. In the case of alumina, an 0.2 g sample exposed to more than 100 ppm of ozone yielded a turnover number of about 0.5 when ozone wall losses were accounted for.

Discussion

O_3 Uptake on α-Fe_2O_3. The uptake of ozone by α-Fe_2O_3 surfaces leads to irreversible loss of gas-phase O_3 where any gas-phase product species are likely to be IR-inactive (e.g., O_2). Additionally, no spectroscopic signatures due to surface-adsorbed products were detected. The ozone turnover numbers listed for the IR probe experiments in Table 1 are in the range $T_N \approx 2-3$, depending on the initial pressure. Higher ozone pressure and lower hematite mass conditions yielded turnover numbers that were an order of magnitude larger, >25. These observations strongly suggest that the uptake is not saturated and that the decomposition process is catalytic under our experimental conditions. A simple mechanism for the catalytic destruction of ozone on metal oxides has been proposed to proceed through generation of a surface oxide species:[28,29]

$$S + O_3 \rightarrow S{-}O + O_2 \quad (4)$$

where S represents an active site and S−O represents the product surface oxide. This step is followed by regeneration of the active site via subsequent reaction with gaseous ozone

$$S{-}O + O_3 \rightarrow S{-}O_2 + O_2 \quad (5)$$

$$S{-}O_2 \rightarrow S + O_2 \quad (6)$$

or recombination of the surface oxide species:

$$2(S{-}O) \rightarrow 2S + O_2 \quad (7)$$

The regeneration steps would make the overall surface reaction catalytic. Roscoe and Abbatt[20] detected an IR absorption feature on alumina films exposed to ozone that could be evidence for the formation of a surface oxide species, as in reaction 4 or 5. Raman spectroscopy was used to characterize a surface peroxide intermediate, formed in reaction 5, for ozone decomposition on a manganese oxide catalyst.[28,29] The catalytic nature of the O_3 decomposition on α-Fe_2O_3 that we observe confirms our previous laboratory studies.[13,14]

We determine an uptake coefficient under dry conditions of $\gamma \approx 10^{-7}$, a value that is found to decrease with increased RH. For comparison, our Knudsen cell studies measured an initial uptake coefficient of $\gamma \approx 10^{-4}$ at much lower O_3 pressures, on the order of 8 ppb.[13,14] The initial uptake is found to decrease as the powder sample becomes increasingly exposed to ozone, consistent with the trend we observe in the present experiments, which employ larger ozone concentrations and, hence, higher surface coverages. Abbatt and co-workers[19] investigated the uptake of ozone by authentic Saharan dust samples and measured a dry uptake coefficient of 2×10^{-7} for an initial ozone pressure of a few parts per million. Hanisch and Crowley[17] measured a steady-state uptake of $\gamma \approx 10^{-5}$ on their Saharan dust sample using a Knudsen cell technique and ozone pressures of approximately 30 ppb. These investigators also noted a strong dependence of the uptake on initial O_3 pressure. Extrapolating their data to a pressure of 20 ppm, typical of our IR experiments, predicts an uptake of $\gamma \approx 10^{-7}$ for the dust sample. Thus, our results are in accord with previous measurements for hematite and actual dust samples when differences due to pressure and coverage are taken into account, and would seem to be representative of ozone interactions with aged, or processed, hematite particles in the atmosphere.

The measured uptake coefficients for lower initial ozone pressures are approximately the same as in the higher concentration experiments. The calculated turnover numbers are less than

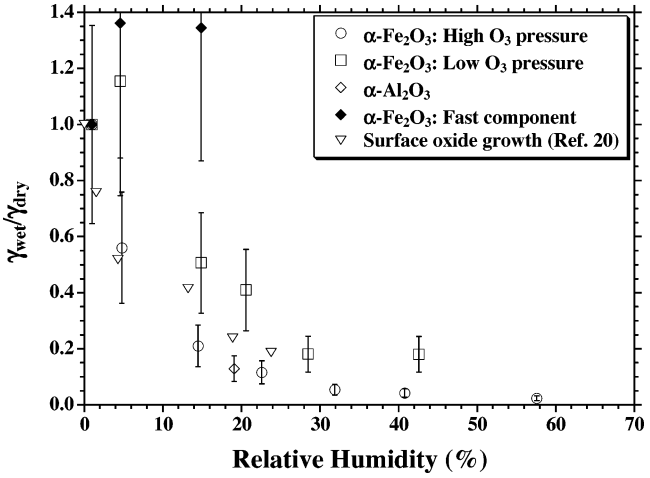

Figure 7. Plot of the ratio $\gamma_{wet}/\gamma_{dry}$ as a function of RH for α-Fe_2O_3, showing both the FT−IR and UV/vis data sets. The ratio for the α-Al_2O_3 data and fast decay component observed in the UV/vis α-Fe_2O_3 data are also shown. A corresponding ratio for rate constants measured for the appearance of a surface product species in ref 20 is included.

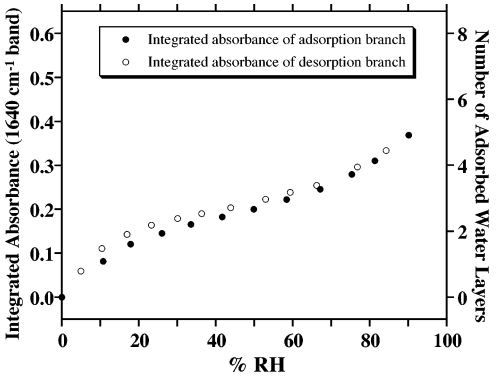

Figure 8. Water isotherm [(●) adsorption curve, (○) desorption curve] on α-Fe_2O_3 at $T = 295$ K. Data are from ref 30.

unity, but all of the O_3 is consumed and the process is still likely catalytic at these lower pressures. We have noted evidence for a faster O_3 loss component in the measured decay curves, corresponding to an uptake coefficient approximately 3−5 times larger than those reported in Table 1 for dry conditions. The fast component may be suggestive of site heterogeneity where some sites on the α-Fe_2O_3 surface are more reactive than others toward ozone. Similar uptake behavior was noted in the case of O_3 reactions with Saharan dust where the faster component yielded a larger uptake coefficient by a factor of 2−3.[19] However, in our experiments with α-Fe_2O_3 this fast pathway must quickly saturate at a coverage of only about 3×10^{13} ozone molecules cm^{-2}. Such a fast, low-coverage process is consistent with higher initial uptake observed in Knudsen cell experiments.[13,14,17] Hanisch and Crowley[17] also concluded that their Saharan dust samples became inactive toward further O_3 decomposition but at higher coverages of about 2×10^{14} ozone molecules cm^{-2}.

The results of our study of RH effects, for both the high and low initial O_3 pressure experiments, clearly show a strong inhibition of ozone decomposition as the RH inside the chamber is increased. The effect of humidity on the uptake coefficient can be conveniently represented as the ratio of the coefficient at a given RH value to the uptake coefficient for the dry, ≤1% RH, experiment, $\gamma_{wet}/\gamma_{dry}$. This ratio is part of Table 1 and is also plotted as a function of RH in Figure 7 for both ozone data sets. The trend is very similar for either low or high initial O_3 pressures, although the effect appears to be stronger for the higher pressure, higher coverage experiments. Furthermore, the RH effect at higher O_3 pressures does not appear to saturate and the ozone decomposition rate continues to decrease up to the highest RH values we have investigated.

In previous studies of ozone uptake on alumina and authentic Saharan dust samples by Abbatt and co-workers,[18,19] little or no dependence of the uptake coefficient on RH was found. In those experiments, like the present report, the loss of the gas-phase ozone reactant was monitored. In a separate experiment by Roscoe and Abbatt,[20] diffuse reflectance IR was utilized to follow the growth of a spectral feature on the surface of an alumina film ascribed to the product of the ozone reaction. In contrast to the previous conclusions, the surface feature was observed to grow in much more slowly as the RH was increased. The ratio of the rate constant for product oxide formation at a particular RH to the dry rate was calculated from Figure 5 of ref 20, and the results are included with our data in Figure 7. The overall decrease in the growth rate as RH is increased follows the trends we observe for the reduction in the uptake coefficient. We note that the Roscoe and Abbatt results in Figure 7 were obtained with similar ozone pressures to previous experiments that found no effect of RH on O_3 uptake. Thus, any discrepancies are not simply due to pressure or coverage effects.

We have also calculated a similar ratio for the fast initial uptake observed in several of the experiments conducted with lower initial ozone concentrations and have included the results in Figure 7. Although the data are noisy, due to the small contribution to the overall decay made by the fast component, it appears that there is no strong dependence on the RH, at least up to 15% RH. For lower RH values, where the water coverage is expected to be submonolayer (vide infra), the adsorbed water molecules do not appear to saturate the active sites on the α-Fe_2O_3 surface that are responsible for the fast ozone uptake process.

Further insight into the role of RH on ozone decomposition in this system may be gained from a consideration of water uptake by α-Fe_2O_3. In Figure 8 we show isotherm data we have collected for water uptake on hematite films from IR measurements of spectral bands due to adsorbed water recorded at different RH values.[30] Coverages were determined with a three-parameter BET fit.[31] The results are characteristic of a BET isotherm with monolayer coverage achieved at approximately 10% RH and multilayer coverages forming for higher RH values. In addition, the uptake coefficient for water on Saharan dust has been measured to be in the range $\gamma \approx 0.02-0.04$,[32] much larger than the corresponding uptake values we have determined for ozone on hematite. Thus, the hematite aerosol will rapidly come to equilibrium with the water vapor as the dust is introduced into the chamber, at a coverage indicated by the isotherm of Figure 8, and the subsequent, much slower, uptake of O_3 will be to an equilibrated, water-coated surface.

The isotherm data of Figure 8 and the summary results of the RH dependence in Table 1 and Figure 7 suggest that H_2O and O_3 molecules compete for the same reactive surface sites on the α-Fe_2O_3, at least for the major ozone loss pathway. Due to the much more rapid uptake of water, there are fewer sites available for ozone and the apparent O_3 uptake is reduced as the RH is increased up to 10−15% RH, when a water monolayer begins to form. A more detailed mechanism for ozone decom-

position would include adsorption, desorption, and surface reactions steps, as follows:

$$S + O_3 \xrightarrow{k_{adsorption}} S{-}O_3 \quad (8)$$

$$S{-}O_3 \xrightarrow{k_{desorption}} S + O_3 \quad (9)$$

$$S{-}O_3 \xrightarrow{k_{reaction}} P \quad (10)$$

If it is assumed that surface reaction, reaction 10, is rate−limiting, then the overall rate will depend on the concentration of surface-adsorbed ozone, which in turn depends on the amount of water coverage. If the surface coverages of ozone and water are expressed as Langmuir-type isotherms, which is reasonable for the low-RH water data, then the overall rate will scale with the pressures of ozone, P_{O_3}, and water, $P_{H_2}O$, as

$$\text{rate} \propto \frac{P_{O_3}}{P_{H_2O}} \quad (11)$$

Equation 11 simply reflects the presence of water on the hematite surface, reducing the number of reactive sites available for the ozone reaction. Since the water concentration in the chamber is constant over the course of the reaction, the ozone decay will still follow first-order kinetics but with a rate that is inversely dependent on the RH. The fast initial uptake of O_3 that we have also observed may be mediated by surface sites that are not initially occupied by water molecules and, as a result, the decay appears to be RH-independent. Note that the uptake coefficient for the fast O_3 component is still much smaller than that expected for water uptake to the α-Fe_2O_3 surface. However, as the RH reaches 10−15%, a monolayer of water is formed, potentially blocking all of the sites and cutting off the fast decay pathway. Indeed, the fast component cannot be discerned for RH values above 15%.

Infrared spectroscopic studies of adsorption on various metal oxides reveal that ozone binds strongly to Lewis acid sites on oxides, which arise due to coordinatively unsaturated metal ions.[33,34] Binding at these sites distorts the ozone molecular geometry, presumably leading to decomposition and formation of a surface oxide. Blocking of the acid sites suppresses ozone binding and decomposition. For example, on fully hydrated TiO_2 surfaces, no strongly bound ozone is observed. When the surface is partially dehydrated, generating Lewis acid sites, spectral features due to strongly bound O_3 reappear. Ozone decomposition on alumina surfaces can be completely suppressed by coadsorption of a base, such as pyridine.[35]

As the RH increases beyond 10−15%, multilayer water coverage is indicated by Figure 8, reaching approximately 2 monolayers by 30% RH. However, ozone continues to react at these higher RH values, albeit at a slower rate, and ozone turnover numbers are still greater than unity. The effect of RH in reducing ozone uptake does not appear to saturate, at least for the higher ozone concentration data, and the apparent uptake continues to decrease up to 58% RH. These experimental observations are inconsistent with a simple site-blocking argument for the effect of adsorbed water on ozone uptake, which would predict a significant decrease in O_3 uptake once a water monolayer forms and no further changes for higher water coverage. An alternative mechanism, whereby ozone must displace adsorbed water from a reactive surface site for the reaction to proceed, appears unlikely for the same reason; once a monolayer forms and all of the surface sites are occupied by water, the rate of displacement would reach some limiting value. In contrast, the experimental data show decreasing rates of O_3 loss at RH values beyond the predicted formation of a water monolayer.

The amount of water adsorbed onto the surface of the hematite particulates may be sufficiently large that it is liquidlike in its physical and chemical properties. For example, there is spectroscopic evidence suggesting that adsorbed water has a bulk, liquidlike environment with as few as 2 monolayers on some substrates.[36] In that case, it may be more appropriate to represent ozone uptake by a resistance model. The resistance model expresses the measured uptake as a sum of terms due to mass accommodation, liquid solubility, and aqueous phase reaction:[1]

$$\frac{1}{\gamma} = \frac{1}{\alpha} + \frac{1}{\gamma_{sol} + \gamma_{rxn}} \quad (12)$$

where α is the mass accommodation coefficient, γ_{sol} is the solubility-limited uptake coefficient, and γ_{rxn} is the reactive uptake coefficient. Gas-phase diffusion has been neglected in eq 12, as it is unimportant given the small uptake coefficients measured and the relatively small dust particles used. The mass accommodation coefficient for ozone on liquid water is probably $\alpha > 0.1$,[37,38] orders of magnitude larger than the apparent uptake coefficients we have measured at higher RH. Thus, according to the resistance model, ozone uptake is limited by either solubility or reaction in the liquidlike layer. The solubility-limited uptake coefficient depends on the diffusion length, $\sqrt{Dt}$,[1] where D is the diffusion coefficient for O_3 in water (1.85×10^{-5} cm^2 s^{-1})[39] and t is the gas−liquid contact time. Given the long exposure times in our experiment and the thin water layer formed, the diffusion length will be relatively long and a liquidlike layer would be saturated. Thus, solubility would not limit the uptake process. According to Henry's law, the aqueous ozone concentration is given by

$$[O_3] = HP_{O_3} \quad (13)$$

where H is the Henry's law constant for ozone (1.15×10^{-2} M atm^{-1})[40] and P_{O_3} is the gas-phase ozone pressure. For a mean ozone pressure of approximately 20 ppm, the aqueous ozone concentration would be $[O_3] \approx 2 \times 10^{-7}$ M.

These considerations suggest that uptake is limited by aqueous phase reaction. The reaction-limited uptake coefficient is expressed as

$$\gamma_{rxn} = \frac{4HRT}{\bar{c}}\sqrt{k'D} \quad (14)$$

where k' is the pseudo-first-order rate constant for ozone reaction. Using the values for the Henry's law constant and the ozone diffusion coefficient given above, then the measured uptake coefficient at 58% RH, $\gamma \approx 2 \times 10^{-9}$, corresponds to a rate constant of $k' \approx 2 \times 10^{-4}$ s^{-1}. A diffusion-limited rate constant for ozone reaction in bulk water, given the Henry's law concentration above, would be almost 10^7 times larger. As the surface water layer saturates and the reaction step becomes rate-limiting, the O_3 decay will exhibit zero-order kinetics, which is suggested by the near-linear decay of the 58% RH data in Figure 4.

The resistance model, however, does not contain any explicit rationalization for the continued decrease in the ozone uptake as the RH is increased, as exemplified by the data of Figure 7. It may be that there is some transitional behavior between dry conditions and a higher RH environment before a liquidlike layer

forms that is difficult to describe quantitatively. The pH of colloidal hematite solutions is approximately 8.1−8.5 and the rate of ozone decomposition in water is known to increase with pH due to reaction with hydroxide ions. At a pH of 8.5, the half-life of ozone is approximately 20 min.[41] As a consequence, one might actually expect the ozone uptake to increase as a water layer forms on the hematite surface.

Alternatively, it may be that water adsorption is not uniformly distributed on the surface of the hematite particles. The water may preferentially cluster on the surface, leaving bare hematite surface that can react with ozone but yielding a lower measured uptake due to the reduced number of available surface sites. For example, the measured ratio $\gamma_{wet}/\gamma_{dry}$ at 23% RH implies that about 12% of the hematite surface is open despite the expectation from Figure 8 that the water coverage is 2 monolayers. The surface may not be completely covered until higher RH values of 60% or so, then forming a liquidlike water layer that makes the resistance model, above, a good descriptor of the ozone decomposition process. Infrared probes of water uptake by nitrated α-Al_2O_3 powders in our laboratory show spectroscopic evidence for both oxide-coordinated and water-solvated surface nitrate, suggesting that the water coverage is nonuniform at RH values corresponding to monolayer coverage.[31] Sum frequency generation (SFG), a surface-sensitive nonlinear spectroscopic technique, was used to detect isolated, non-hydrogen-bonded surface hydroxyl sites on α-Al_2O_3 at even higher RH, 54%, where the expected water coverage is ≈3 monolayers.[42] Similar evidence from SFG spectra was found for water clustering on silica surfaces.[42] Water uptake to another metal oxide, MgO, appears to yield three-dimensional islands (i.e., with multilayer thickness) prior to coalescence and eventual surface saturation.[43,44]

Another possible scenario is that the water layer formed on the surface is not liquidlike at all. Interactions between adsorbed water molecules and the hematite surface could yield a strongly polarized water layer that forms a relatively rigid framework, making ozone diffusion very slow. As the water layer increases in thickness at higher RH, the rate of ozone diffusion through the ordered layers decreases and the measured uptake would be lower. Indeed, there is ample suggestion from surface studies that monolayer water adsorption on certain substrates can form a more structured, ice-like layer.[43,45,46] Generally, subsequent water overlayers may not be as strongly polarized by the surface and manifest a more disordered environment, suggestive of liquid water-like behavior. However, our work with α-Al_2O_3 crystals indicates that the adsorbed water can still be highly ordered even for RH values of ≈70%, corresponding to a measured coverage of 4−5 monolayers.[45] Similarly, recent work on silica surfaces suggests multilayer formation of structured ice-like water.[47] Given that the water layer thickness is very small for, say, 2 monolayers, about 6 Å, and that the contact time in our experiments is very long, consideration of the characteristic diffusion length, $\sqrt{Dt}$, implies that the diffusion coefficient for ozone in the water layer would have to be exceedingly small.

O_3 Uptake on α-Al_2O_3. The data of Figure 6 clearly show that uptake of ozone by alumina is less than by the hematite sample, yielding an uptake coefficient of $\gamma = 3.5 \times 10^{-8}$ under dry conditions, approximately 3 times less than the hematite uptake under the same conditions. More importantly, perhaps, the uptake is observed to saturate with a turnover number of about 1 and only about a quarter of the initial ozone reacted by the end of the experiment (Table 1). Even with a considerable excess of available ozone, the calculated turnover number does not increase and is still less than 1. Thus, it would appear that ozone decomposition on α-Al_2O_3 is not catalytic and saturates at a coverage of about $(2-4) \times 10^{14}$ ozone molecules cm^{-2}. This observation may appear somewhat surprising as both hematite and alumina have, at least, similar surface functionality with terminal hydroxyl groups. However, while ozone can hydrogen-bond to the surface hydroxyls, ozone decomposition likely takes place at more reactive surface sites, including defects.[33−35] These sites may exhibit very different reactivities in hematite and alumina due to the different electronic structure of the respective metal centers. For example, it has been shown that α-Fe_2O_3 exhibits a stronger affinity for binding certain metal complexes than α-Al_2O_3.[48,49]

We measured a value of $\gamma \approx 10^{-4}$ for alumina in our Knudsen cell work[13] but at much lower pressures, 8 ppb O_3. Abbatt and co-workers[18] determined a smaller uptake, $\gamma \approx 10^{-6}$, at higher initial ozone concentration of ≈4 ppm. The latter uptake measurement is more in accord with our study but still significantly higher. The Saharan dust samples studied by Hanisch and Crowley[17] contained about 18% alumina. Extrapolation of their results, obtained under dry conditions, yields an uptake coefficient of $\gamma \approx 10^{-7}$, closer to our value. Both of these latter groups noted that the alumina surface saturated, preventing further ozone decomposition, at coverages of $(1.4-2.1) \times 10^{14}$ molecules cm^{-2}, somewhat lower than the coverages estimated in our study but nevertheless suggesting a lack of catalytic activity. The experiments of Hanning-Lee et al.[21] yielded ozone uptake values of $\gamma \approx 3 \times 10^{-10}$ for alumina at much higher initial O_3 pressures. They also reported that both H_2O and HCl adsorption resulted in a slower rate of ozone decomposition, although these conclusions were not quantified.

The RH dependence of the alumina uptake is, however, quite similar to the hematite case, exhibiting a significant decrease in apparent ozone uptake as the RH is increased. At 56% RH, the ozone decay exhibits zero-order kinetics and was not well fit to an exponential function. The ratio $\gamma_{wet}/\gamma_{dry}$ for alumina has been calculated and plotted in Figure 7. The data for α-Al_2O_3 follow the general trend of the hematite data.

Atmospheric Implications. The ozone uptake coefficients measured for hematite in the present study are not large relative to more typical homogeneous loss pathways. The uptake recorded for alumina is even smaller. Furthermore, we find that the uptake is significantly inhibited due to the presence of adsorbed water at RH values that are more typical of the ambient troposphere. Although the uptake coefficient is larger at lower ozone pressures, more characteristic of the real atmosphere, the decomposition rate is still small. Overall, the results suggest that, for clean surfaces, ozone loss due to mineral dust may not be significant. However, in the atmosphere, the presence of other reactive trace gas species will likely result in a modified dust surface. Thus, observed correlations between ozone loss and dust concentration may derive from the presence of reactive coadsorbates or different surface functional groups on aged dust particles. In addition, the catalytic nature of the hematite dust surface toward ozone decomposition needs to be taken into account when attempting to model the results of field observations. The mineral dust aerosol itself may be chemically altered by exposure to ozone. Oxidation of the surface could make the dust more hydrophilic, leading to increased water uptake. The resultant physical changes, such as particle growth and changes in optical constants, could have implications for radiative forcing. Such surface modifications might enhance atmospheric aqueous-phase chemistry due to the growth of a liquid water shell around the mineral dust core.

Conclusions

We have measured the kinetics of ozone uptake onto representative mineral dust samples, α-Fe_2O_3 and α-Al_2O_3, in an environmental reaction chamber. The uptake coefficient for hematite under dry conditions was found to be $\gamma = 1.0 \times 10^{-7}$, and the alumina uptake was smaller by about a factor of 3. While the decomposition process is catalytic on the hematite surface, the reaction on alumina becomes saturated and is apparently not catalytic. For both samples, increasing the RH resulted in a strong decrease in the measured ozone uptake up to the highest RH investigated, approximately 60%. Under these conditions, the water coverage is approximately 2−3 monolayers. Possible explanations for the observed RH dependence are discussed.

Acknowledgment. This material is based upon work supported by the National Science Foundation under Grants CHE-9984344 and CHE-0503854. Any opinions, findings, and conclusions or recommendations expressed in this material are those of the authors and do not necessarily reflect the views of the National Science Foundation. We thank Jonas Balustratis for making the water uptake measurements on hematite.

References and Notes

(1) Kolb, C. E.; Worsnop, D. R.; Zahniser, M. S.; Davidovits, P.; Hanson, D. R.; Ravishankara, A. R.; Keyser, L. F.; Leu, M.-T.; Williams, L. R.; Molina, M. J.; Tolbert, M. A. Laboratory Studies of Atmospheric Heterogeneous Chemistry. In *Progress and Problems in Atmospheric Chemistry*; Barker, J. R., Ed.; World Scientific: River Edge, NJ, 1995; Vol. 3.

(2) Andreae, M. O.; Crutzen, P. J. *Science* **1997**, *276*, 1052.

(3) Molina, M. J.; Molina, L. T.; Kolb, C. E. *Annu. Rev. Phys. Chem.* **1996**, *47*, 327.

(4) Kreidenweis, S. *Perspectives in Environmental Chemistry*; University Press: New York, 1998.

(5) Ravishankara, A. R. *Science* **1997**, *276*, 1058.

(6) Finlayson-Pitts, B. J.; Hemminger, J. C. *J. Phys. Chem. A* **2000**, *104*, 11463.

(7) Grassian, V. H. *Int. Rev. Phys. Chem.* **2001**, *20*, 467.

(8) Usher, C. R.; Michel, A. E.; Grassian, V. H. *Chem. Rev.* **2003**, *103*, 4883.

(9) de Reus, M.; Dentener, F.; Thomas, A.; Borrmann, S.; Strom, J.; Lelieveld, J. *J. Geophys. Res.* **2000**, *105*, 15263.

(10) Dentener, F. J.; Carmichael, G. R.; Lelifeld, J.; Zhang, Y.; Crutzen, P. *J. Geophys. Res.* **1996**, *101*, 22869.

(11) Zhang, Y.; Sunwoo, Y.; Kotamarthi, V.; Carmichael, G. R. *J. Appl. Meteorol. (1988)* **1994**, *33*, 813.

(12) Prospero, J. M.; Schmitt, R.; Cuevas, E.; Savoie, D. L.; Graustein, W. C.; Turekian, K. K.; Volz-Thomas, A.; Diaz, A.; Oltmans, S. J.; Levy, H., II. *Geophys. Res. Lett.* **1995**, *22*, 2925.

(13) Michel, A. E.; Usher, C. R.; Grassian, V. H. *Geophys. Res. Lett.* **2002**, *29*, 1669; http://dx.doi.org/10.1029/2002GL014896.

(14) Michel, A. E.; Usher, C. R.; Grassian, V. H. *Atmos. Environ.* **2003**, *37*, 3201.

(15) Al-Abadleh, H. A.; Grassian, V. H. *Surf. Sci. Rep.* **2003**, *52*, 63.

(16) Usher, C. R.; Michel, A. E.; Stec, D.; Grassian, V. H. *Atmos. Environ.* **2003**, *37*, 5337.

(17) Hanisch, F.; Crowley, J. N. *Atmos. Chem. Phys.* **2003**, *3*, 119.

(18) Sullivan, R. C.; Thornberry, T.; Abbatt, J. P. D. *Atmos. Chem. Phys.* **2004**, *4*, 1301.

(19) Chang, R. Y. W.; Sullivan, R. C.; Abbatt, J. P. D. *Geophys. Res. Lett.* **2005**, *32*, L14815; http://dx.doi.org/10.1029/2005GL023317.

(20) Roscoe, J. M.; Abbatt, J. P. D. *J. Phys. Chem. A* **2005**, *109*, 9028.

(21) Hanning-Lee, M. A.; Brady, B. B.; Martin, L. R.; Syage, J. A. *Geophys. Res. Lett.* **1996**, *23*, 1961.

(22) Prince, A. P.; Wade, J.; Grassian, V. H.; Kleiber, P.; Young, M. A. *Atmos. Environ.* **2002**, *36*, 5729.

(23) Orphal, J. *J. Photochem. Photobiol. A* **2003**, *157*, 185.

(24) Hanst, P. L.; Stephens, E. R.; Scott, W. E.; Doerr, R. C. *Anal. Chem.* **1961**, *33*, 1113.

(25) McAfee, J. M.; Stephens, E. R.; Fitz, D. R.; Pitts, J. N., Jr. *J. Quant. Spectrosc. Radiat. Transfer* **1976**, *16*, 829.

(26) Liang, L.; Morgan, J. J. *Aquat. Sci.* **1990**, *52*, 32.

(27) Knoezinger, H.; Ratnasamy, P. *Catal. Rev.*—Sci. Eng. **1978**, *17*, 31.

(28) Li, W.; Oyama, S. T. *J. Am. Chem. Soc.* **1998**, *120*, 9047.

(29) Li, W.; Gibbs, G. V.; Oyama, S. T. *J. Am. Chem. Soc.* **1998**, *120*, 9041.

(30) Balustratis, J.; Grassian, V. H. Unpublished results, 2006.

(31) Goodman, A. L.; Bernard, E. T.; Grassian, V. H. *J. Phys. Chem. A* **2001**, *105*, 6443.

(32) Seisel, S.; Lian, Y.; Keil, T.; Trukhin, M. E.; Zellner, R. *Phys. Chem. Chem. Phys.* **2004**, *6*, 1926.

(33) Bulanin, K. M.; Lavalley, J. C.; Tsyganenko, A. A. *J. Phys. Chem.* **1995**, *99*, 10294.

(34) Bulanin, K. M.; Lavalley, J. C.; Tsyganenko, A. A. *Colloids Surf., A* **1995**, *101*, 153.

(35) Thomas, K.; Hoggan, P. E.; Mariey, L.; Lamotte, J.; Lavalley, J. C. *Catal. Lett.* **1997**, *46*, 77.

(36) Peters, S. J.; Ewing, G. E. *J Phys. Chem. B* **1997**, *101*, 10880.

(37) Utter, R. G.; Burkholder, J. B.; Howard, C. J.; Ravishankara, A. R. *J. Phys. Chem.* **1992**, *96*, 4973.

(38) Magi, L.; Schweitzer, F.; Pallares, C.; Cherif, S.; Mirabel, P.; George, C. *J. Phys. Chem. A* **1997**, *101*, 4943.

(39) Matrozov, V. I.; Kashtanov, S. A.; Stepanov, A. M.; Tregubov, B. A. *Zh. Prikl. Khim.* **1976**, *49*, 1070.

(40) Chameides, W. L. *J. Geophys. Res.* **1984**, *89*, 4739.

(41) Staehelin, J.; Hoigne, J. *Environ. Sci. Technol.* **1982**, *16*, 676.

(42) Liu, D.; Ma, G.; Xu, M.; Allen, H. C. *Environ. Sci. Technol.* **2005**, *39*, 206.

(43) Ewing, G. E. *Chem. Rev.* **2006**, *106*, 1511.

(44) Foster, M.; D'Agostino, M.; Passno, D. *Surf. Sci.* **2005**, *590*, 31.

(45) Al-Abadleh, H. A.; Grassian, V. H. *Langmuir* **2003**, *19*, 341.

(46) Miranda, P. B.; Xu, L.; Shen, Y. R.; Salmeron, M. *Phys. Rev. Lett.* **1998**, *81*, 5876.

(47) Asay, D. B.; Kim, S. H. *J. Phys. Chem. B* **2005**, *109*, 16760.

(48) Catalano, J. G.; Trainor, T. P.; Eng, P. J.; Waychunas, G. A.; Brown, J. G. E. *Geochim. Cosmochim. Acta* **2005**, *69*, 3555.

(49) Templeton, A. S.; Trainor, T. P.; Traina, S. J.; Spormann, A. M.; Brown, G. E., Jr. *Proc. Natl. Acad. Sci. U.S.A.* **2001**, *98*, 11897.